Transport of short-lived halocarbons to the stratosphere over the Pacific Ocean.

Michal T. Filus[1], Elliot L. Atlas[2], Maria A. Navarro[2*], Elena Meneguz[3], David Thomson[3], Matthew J. Ashfold[4], Lucy J. Carpenter[5], Stephen J. Andrews[5], Neil R.P. Harris[6]

1. Centre for Atmospheric Science, University of Cambridge, Cambridge, CB2 1EW, UK

2. Department of Atmospheric Sciences, RSMAS, University of Miami, Miami, Florida, USA

3. Met Office, Atmospheric Dispersion Group, FitzRoy Road, Exeter, EX1 3PB, UK

4. School of Environmental and Geographical Sciences, University of Nottingham Malaysia, 43500,Semenyih, Selangor, Malaysia

5. Wolfson Atmospheric Chemistry Laboratories, Department of Chemistry, University of York, York, YO10 5DD, UK

6. Centre for Environmental and Agricultural Informatics, Cranfield University, Cranfield, MK43 0AL, UK

Correspondence to: Neil Harris (neil.harris@cranfield.ac.uk)

Abstract. The effectiveness of transport of short-lived halocarbons to the upper troposphere and lower stratosphere remains an important uncertainty in quantifying the supply of ozone-depleting substances to the stratosphere. In early 2014, a major field campaign in Guam in the West Pacific, involving UK and US research aircraft, sampled the tropical troposphere and lower stratosphere. The resulting measurements of CH_3I, $CHBr_3$ and CH_2Br_2 are compared here with calculations from a Lagrangian model. This methodology benefits from an updated convection scheme which improves simulation of the effect of deep convective motions on particle distribution within the tropical troposphere. We find that the observed CH_3I, $CHBr_3$ and CH_2Br_2 mixing ratios in the Tropical Tropopause Layer (TTL) are consistent with those in the boundary layer when the new convection scheme is used to account for convective transport. More specifically, comparisons between modelled estimates and observations of short-lived CH_3I indicate that the updated convection scheme is realistic up to the lower TTL but is less good at reproducing the small number of extreme convective events in the upper TTL. This study consolidates our understanding of the transport of short-lived halocarbons to the upper troposphere and lower stratosphere by using improved model calculations to confirm consistency between observations in the boundary layer, observations in the TTL, and atmospheric transport processes. Our results support recent estimates of the contribution of short-lived bromocarbons to the stratospheric bromine budget.

1 Introduction

The successful implementation of the Montreal Protocol with its adjustments and amendments has led to reductions in stratospheric chlorine and bromine amounts since the late 1990s (Carpenter et al., 2014). These reductions have halted the ozone decrease (Harris et al., 2015; Chipperfield et al., 2017; Steinbrecht et al., 2017) with the exception of the possible reduction in the lower stratosphere (Ball et al., 2017; Chipperfield et al., 2018; Ball et al., 2019). Recently, the importance of very short-lived (VSL) chlorine- and bromine containing compounds has received a great deal of attention (e.g. Hossaini et al., 2017; Oram et al., 2017). VSLS are not controlled under the Montreal Protocol, but

*Deceased: 19.12.2017

43 are required in order to reconcile observed stratospheric measurements of inorganic or 'active'
44 bromine with reported anthropogenic bromine emission sources. However VSLS input into the
45 stratosphere has remained a poorly constrained quantity (Carpenter et al., 2014), which hinders our
46 understanding of the on-going decline in lower stratospheric ozone and our ability to make
47 predictions of stratospheric ozone recovery.

48 Three of the most important VSL halocarbons are: methyl iodide, CH_3I; bromoform, $CHBr_3$; and
49 dibromomethane, CH_2Br_2. They have typical lower tropospheric lifetimes (4, 15 and 94 days,
50 respectively (Carpenter et al., 2014)) which are shorter than tropospheric transport timescales and so
51 they have non-uniform tropospheric abundances. They are emitted predominantly from the oceans
52 and result principally from natural sources (e.g. Lovelock, 1975; Moore et al., 1995; Oram and
53 Penkett, 1994; Vogt et al., 1999; Pyle et al., 2011; Carpenter et al.,1999, 2012, 2014; Tegtmeier et
54 al., 2013; Saiz-Lopez et al., 2014). The short-lived bromocarbons, chiefly $CHBr_3$ and CH_2Br_2, have
55 been identified as the missing source for stratospheric bromine (the sum of bromine atoms in long-
56 lived brominated organic and inorganic substances; Pfeilsticker et al., 2000; Feng et al., 2007;
57 Dessens et al., 2009). The current estimate of the contribution of the short-lived bromocarbons to the
58 active bromine (Br_y) in the stratosphere is ~5 (3-7) ppt (Engel et al., 2018), which is slightly
59 narrower than the previous range of 3-8 ppt (Liang et al., 2010, 2014; Carpenter et al., 2014;
60 Fernandez et al., 2014; Sala et al., 2014; Tegtmeier et al., 2015; Navarro et al., 2015, 2017; Hossaini
61 et al., 2016; Butler et al., 2017; Fiehn et al., 2017). Much of the uncertainty is linked to the
62 contribution of $CHBr_3$ which has both the shortest lifetime and the largest emissions of the
63 commonly observed bromocarbons.

64 The transport of VSL halocarbons into the lower stratosphere is by ascent through the tropical
65 tropopause layer (TTL) (Fueglistaler et al., 2009). An important factor influencing the loading of the
66 VSL bromocarbons in the TTL is the strength of the convective transport from the boundary layer
67 where the bromocarbons are emitted (Hosking et al., 2010; Yang et al., 2014; Russo et al., 2015;
68 Hepach et al., 2015; Fuhlbrügge et al., 2016; Krzysztofiak et al., 2018). This is poorly quantified and,
69 when taken together with the large variations in boundary layer concentrations and the uncertainties
70 associated with the model representation of convection, limits our ability to model the bromine
71 budget in the current and future atmosphere (Liang et al., 2010, 2014; Hoyle et al., 2011; Russo et
72 al., 2011, 2015; Schofield et al., 2011; Aschmann et al., 2013; Fernandez et al., 2014; Hossaini et al.,
73 2016; Krzysztofiak et al., 2018).

74 To address this and other challenges, the Natural Environment Research Council Coordinated
75 Airborne Studies in the Tropics (NERC CAST), National Centre for Atmospheric Research
76 Convective Transport of Active Species in the Tropics (NCAR CONTRAST) and National
77 Aeronautics and Space Administration Airborne Tropical Tropopause Experiment (NASA
78 ATTREX) projects were organised (Harris et al., 2017; Jensen et al., 2017; Pan et al., 2017). These
79 projects joined forces in January-March 2014 in the American territory of Guam, in the West Pacific.
80 Three aircraft were deployed to sample air masses at different altitudes to investigate the
81 characteristics of air masses influenced by deep convection. This campaign produced a unique
82 dataset of coordinated measurements for interpretative studies of transport and distribution of the
83 chemical species, including the VSL bromocarbons (Sect. 2.1 and 2.2). The NASA ATTREX project
84 also measured over the less convectively active east Pacific in January - February 2013.

The objective of this paper is to model the transport and distribution of CH_3I, $CHBr_3$ and CH_2Br_2 in the TTL by quantifying their boundary layer and background contribution components using a Lagrangian methodology building on the approach of Ashfold et al (2012). A new parameterisation scheme of convection for the NAME trajectory model is used with the short-lived CH_3I serving as an excellent way to assess the performance of the new scheme. Briefly, the approach uses clusters of back trajectories starting at measurement points to quantify how much of CH_3I, $CHBr_3$ and CH_2Br_2 in the TTL come from the boundary layer, thereby assessing the role of convection in transporting these compounds to the TTL. The calculation is completed by estimating the background component (i.e. how much of CH_3I, $CHBr_3$ and CH_2Br_2 originate from outside the immediate boundary layer source). Section 2 presents an overview of the field campaigns, the CH_3I, $CHBr_3$ and CH_2Br_2 measurements, and how the NAME calculations are used. In Section 3, the approach is illustrated by comparing model estimates and measurements from one ATTREX 2014 flight. This analysis is then expanded to cover measurements from all ATTREX 2014 and 2013 flights. The role of convection in transporting VSL halocarbons to the TTL is further examined in Section 4. Based on the modelled calculations of $CHBr_3$ and CH_2Br_2, Section 5 discusses how much these VSL bromocarbons contribute to the bromine budget in the TTL.

2 Methodology

2.1 Overview of the CAST, CONTRAST and ATTREX campaigns

The joint CAST, CONTRAST and the third stage of the ATTREX campaign took place in January-March 2014, in the West Pacific. Guam (144.5^o E, 13.5^o N) was used as a research mission centre for these three campaigns. Three aircraft were deployed to measure physical characteristics and chemical composition of tropical air masses from the earth's surface up to the stratosphere. In CAST, the Facility for Airborne Atmospheric Measurements (FAAM) BAe-146 surveyed the boundary layer and lower troposphere (0-8 km) to sample the convection air mass inflow, while in CONTRAST the National Science Foundation - National Center for Atmospheric Research (NSF-NCAR) Gulfstream V (GV) principally targeted the region of maximum convective outflow in the mid- and upper troposphere, and sampled down to the boundary layer on occasion (1-14 km). Finally, in ATTREX, the NASA Global Hawk (GH) sampled the TTL (13-20 km) to cover air masses likely to be detrained from the higher convective outflow. For more details on these campaigns and the objectives, meteorological conditions and descriptions of individual flights, please refer to the campaign summary papers: Harris et al., 2017 (CAST), Pan et al., 2017 (CONTRAST) and Jensen et al., 2017 (ATTREX). ATTREX had four active measurement campaigns, and we also consider the second campaign which was based in Los Angeles in January-March 2013 and which extensively sampled the East and Central Pacific TTL in six research flights.

2.2 Measurements of the VSL halocarbons

Whole Air Samplers (WAS) were deployed on all three aircraft to measure VSL halocarbons. The FAAM BAe-146 and NSF-NCAR GV also used on-board gas chromatography-mass spectrometry (GC-MS) system for real-time analysis (Wang et al., 2015; Andrews et al., 2016; Pan et al., 2017), though these measurements are not used in our analysis. WAS instrumentation is well established and has been used routinely in previous deployments. The sampling and analytical procedures are capable of accessing a wide range of mixing ratios at sufficient precision and the measurements from the three aircraft have been shown to be consistent and comparable (Schauffler et al., 1998; Park et al., 2010; Andrews et al., 2016).

128 The CAST VSL halocarbon measurements were made using the standard FAAM WAS canisters
129 with 30 second filling time. Up to 64 samples could be collected on each flight and these were
130 analysed in the aircraft hangar, usually within 72 hours after collection. Two litres of sample air were
131 pre-concentrated using a thermal desorption unit (Markes) and analysed with GC-MS (Agilent 7890
132 GC, 5977 Xtr MSD). Halocarbons were quantified using a NOAA calibration gas standard. The
133 measurement and calibration technique is further described and assessed in Andrews et al. (2013;
134 2016).

135 The ATTREX AWAS sampler consisted of 90 canisters, being fully automated and controlled from
136 the ground. Sample collection for the AWAS samples was determined on a real-time basis depending
137 on the flight plan altitude, geographic location, or other relevant real-time measurements. The filling
138 time for each canister ranged from about 25 seconds at 14 km to 90 seconds at 18 km. Canisters were
139 immediately analysed in the field using a high performance GC-MS coupled with a highly sensitive
140 electron capture detector. The limits of detection are compound-dependent and vary from ppt to sub-
141 ppt scale, set at 0.01 ppt for $CHBr_3$, CH_2Br_2 and CH_3I (Navarro et al., 2015). A small artefact of
142 ~0.01-0.02 ppt for CH_3I cannot be excluded. AWAS samples collected on the GV were analysed
143 with the same equipment. Detailed comparison of measurements from the three systems found
144 agreement within ~7 % for $CHBr_3$, ~3 % for CH_2Br_2, and 15 % for CH_3I (Andrews et al., 2016).

2.3 UK Meteorological Office NAME Lagrangian Particle Dispersion Model

146 The Lagrangian particle dispersion model, NAME (Jones, et al., 2007), is used to simulate the
147 transport of air masses in the Pacific troposphere and the TTL. Back trajectories are calculated with
148 particles being moved through the model atmosphere using operational analyses (0.352° longitude
149 and 0.235° latitude, i.e. ~25 km, with 31 vertical levels below 19 km) calculated by the
150 Meteorological Office's Unified Model at 3-hour intervals. This is supplemented by a random walk
151 turbulence scheme to represent dispersion by unresolved aspects of the flow (Davies et al., 2005).
152 For this analysis, the NAME model is used with the improved convection scheme (Meneguz and
153 Thomson, 2014) which simulates displacement of particles subject to convective motions more
154 realistically than previously (Meneguz et al., 2019). NAME is run backward in time to determine the
155 origin(s) of air measured at a particular location (WAS sample) along the ATTREX GH flight track.

156 15,000 particles are released from each point along the flight track where VSL halocarbons were
157 measured in WAS samples. To initialise the NAME model, particles are released randomly in a
158 volume with dimensions 0.1° × 0.1° × 0.3 km centred on each sample. As particles are followed 12
159 days back in time, trajectories are filtered on the basis of first crossing into the boundary layer (1
160 km). Subsequently, the fraction of particles which crossed below 1 km is calculated for each WAS
161 measurement point (Ashfold et al., 2012). The NAME 1 km fractions are indicative of the boundary
162 layer air mass influence to the TTL. The 1 km boundary layer fractions are then used to
163 quantitatively estimate the VSL halocarbon contribution to the TTL from the boundary layer,
164 $[X]_{BL\_Contribution}$. In order to compare the measured and modelled halocarbon values, estimates of the
165 contribution from the background troposphere, $[X]_{BG\_Contribution}$ (i.e. air which has not come from the
166 boundary layer within 12 days) are made. The model estimate for the total halocarbon mixing ratio,
167 $[X]_{NAME\_TTL}$, is thus given by Eq. (1):

$$[X]_{NAME_{TTL}} = [X]_{BL\_Contribution} + [X]_{BG\_Contribution} \qquad (1)$$

169 The methods for calculating $[X]_{BL\_Contribution}$ and $[X]_{BG\_Contribution}$ are now described.

170

2.3.1 NAME modelled boundary layer contribution

The contribution from the boundary layer, ($[X]_{BL\_Contribution}$ - described above) to the VSLs in the TTL can be estimated using

   (i)   the fractions of trajectories crossing below 1 km in the previous 12 days;
   (ii) the transport times to the TTL calculated for each particle;
   (iii) the initial concentration values for CH_3I, $CHBr_3$ and CH_2Br_2; and
   (iv) their atmospheric lifetimes (to account for the photochemical removal along the trajectory).

More specifically, the boundary layer contribution to the TTL for the VSL halocarbons is calculated using Eq. (2) and Eq. (3):

$$[X]_{BL_{Contribution},t} = [X]_{BL} \times fraction_t \times exp^{(-t/\tau)} \qquad (2)$$

$$[X]_{BL\_Contribution} = \Sigma\big([X]_{BL_{Contribution},t}\big) \qquad (3)$$

Equation (2) gives the boundary layer contribution to the TTL for a given tracer, X (where X could be CH_3I, $CHBr_3$, CH_2Br_2), at model output time step, t. The model output time step used is 6 hours, from t = 0 (particle release) to t = 48 (end of a 12 day run). $[X]_{BL}$ stands for the initial boundary layer concentration of a given tracer - assigned to each particle which crossed below 1 km (Table 1). $Fraction_t$ is a number of particles which first crossed 1 km in a model output time step, t, over a total number of particles released, and $exp^{(-t/\tau)}$ is a term for the photochemical loss (where τ stands for atmospheric lifetime of a respective VSL halocarbon). Equation (3) gives the boundary layer contribution that is the sum of boundary layer contribution components in all model output time steps (for t = 1 to 48).

Equation (2) calculates the decay of each tracer after it leaves the boundary layer (0-1 km) which is valid for a well-mixed boundary layer. Since 15,000 particles are released for each AWAS sample, contributions from each particle from below 1 km in the previous 12 days are summed. Decay times, τ, of 4, 15 and 94 days for CH_3I, $CHBr_3$ and CH_2Br_2, respectively, are used (i.e. constant chemical loss rate) (Carpenter et al., 2014). Thus, a particle getting to the TTL in 1 day contributes more of a given tracer to that air mass than a particle taking 10 days. Once this chemical loss term was taken into account, the NAME trajectories can be used to calculate the contribution of convection of air masses from the boundary layer within the preceding 12 days.

The initial boundary layer concentrations are derived from the CAST and CONTRAST WAS measurements taken in the West Pacific in the same period of January-March 2014 as for the ATTREX measurements in the TTL (Table 1). These observed means are used in model calculations, and the similarity between them and literature values reported in Carpenter et al. (2014) is seen, with lower values for $CHBr_3$ only.

2.3.2 NAME modelled background contribution

To compare our model results against the AWAS observations, the background contribution, $[X]_{BG\_Contribution}$ (meaning the contribution from the fraction of trajectories which do not cross below 1 km within 12 days) needs to be accounted for. This requires estimates for the fraction of trajectories from the free troposphere, which is (1-$fraction_{BL}$), Eq. (4), and an estimate of the halocarbon mixing ratio in that fraction, $[X]_{BG}$, Eq. (5) i.e.

$$fraction_{BL} = \Sigma(fraction_t) \qquad (4)$$

$$[X]_{BG\_Contribution} = (1 - fraction_{BL}) \times [X]_{BG} \qquad (5)$$

Since each sample has 15,000 back-trajectories associated with it, some of which came from below 1 km and some of which did not, a definition as to which air samples are considered as boundary layer and which are considered background is required. Two approaches are tested which use the NAME

215 calculations to identify AWAS samples in all flights (2013 and 2014) with low convective influence
216 by (i) filtering for air masses with boundary layer fraction values less than 1, 5 or 10 %; or (ii)
217 selecting the lowest 10 % of boundary layer fractions. Then, the CH_3I, $CHBr_3$ and CH_2Br_2 AWAS
218 observations, corresponding to the boundary layer fraction values less than 1, 5 or 10 %, or the
219 lowest 10 % of boundary layer fractions, are averaged to provide CH_3I, $CHBr_3$ and CH_2Br_2
220 background mixing ratios. These two approaches are explored below (Sect. 3.1.2).

2.3.3 The effect of assuming constant lifetimes

222 The lifetimes of the halocarbons are not the same in the boundary layer and the TTL (Carpenter et al,
223 2014). The assumption of constant lifetime in a 12 day trajectory is evaluated by calculating the
224 difference between idealised trajectories which had 2, 4, 6, 8, and 10 days in the boundary layer and
225 10, 8, 6, 4, and 2 days in the upper troposphere. Lifetimes for the boundary layer and for the upper
226 troposphere for each gas were taken from Carpenter et al. (2014). (Lifetimes for higher altitudes are
227 not available therein). The difference found between the two extreme cases are 6% ($CHBr_3$), 3%
228 (CH_2Br_2) and 25% (CH_3I). The assumption is thus valid for the two brominated species.

229 This assumption is more robust than it might seem at first glance. The boundary layer fraction is
230 calculated using 12 day trajectories in which there is little loss of CH_2Br_2 whether a lifetime of 94 or
231 150 days is taken. The most important factor in determining the amount lofted into the TTL is thus
232 the original mixing ratio which is only slightly modulated by the chemical loss in 12 days. The
233 longer lifetime is absorbed implicitly, and taken into account in the background contribution. The
234 same arguments apply for $CHBr_3$, though the effect is a bit larger. The largest difference is seen for
235 CH_3I. However, the difference matters much less for CH_3I because only 4-5% remains after the full
236 12 days which is much smaller than the uncertainties in this analysis so that much shorter trajectories
237 are used to validate the new convection scheme.
238

3 Analysis of ATTREX 2014 Research Flight 02

240 We start by showing our results from a single ATTREX 2014 research flight, RF02, to illustrate the
241 method. This is followed by analysing all research flights together for ATTREX 2014 and 2013 in
242 Sect. 4, and calculating the modelled contribution of active bromine from $CHBr_3$ and CH_2Br_2 to the
243 TTL (Sect. 5).

3.1 Individual ATTREX 2014 Flight: Research Flight 02

245 Figure 1 shows the vertical distribution of CH_3I, $CHBr_3$ and CH_2Br_2 in the TTL observed during
246 research flight, RF02, during ATTREX 2014. Held on 16-17 February 2014, RF02 was conducted in
247 a confined area east of Guam (12-14° N, 145-147° E) due to a faulty primary satellite
248 communications system for Global Hawk command and control (Jensen, et al., 2017). Twenty six
249 vertical profiles through TTL were made, with 86 AWAS measurements taken in total. A high
250 degree of variability of CH_3I in the TTL was observed (from > 0.4 ppt at 14-15 km, to near-zero ppt
251 values at 17-18 km). Each profile, in general, showed a gradation in CH_3I distribution in the TTL.
252 Higher values were measured in the lower TTL up to 16 km, with values decreasing with altitude.
253 The same pattern was observed for $CHBr_3$ and CH_2Br_2, with the highest concentrations measured in
254 the lower TTL (14-15 km), and the lowest at 17-18 km.

3.1.1 NAME modelled boundary layer contribution

256 Figure 2(a) shows the vertical distribution of the boundary layer air contribution to the TTL
257 (corresponding to the AWAS measurement locations along the RF02 flight track). It reveals higher
258 boundary layer air influence in the lower TTL, decreasing with altitude (similarly to the VSL
259 halocarbon observations). Cumulatively, the highest fractions from below 1 km are found for the
260 lower TTL (14-15 km). A noticeable decrease occurs between the lower and upper TTL (15 to 17

261 km). From 16 km up, little influence (indicated by <10 % and <5 % 1 km fractions of trajectories
262 below 1 km for 16-17 km and 17-18 km, respectively) of the low-level air masses is seen.

263 Figure 2(b) shows all NAME runs for RF02 grouped into four 1 km TTL bins: 14-15 km, 15-16 km,
264 16-17 km and 17-18 km. In the 14-15 km bin, most particles from the low troposphere arrived in the
265 preceding 4 days with many in the preceding 2 days. This represents the fast vertical uplift of the low
266 tropospheric air masses to the lower TTL. At 15-16 km, two particle populations are observed: the
267 first group results from recent vertical uplift, while the second group has been in the upper
268 troposphere for longer than a couple of days (see Fig. 2c in Navarro et al., 2015 for similar example).
269 Above 16 km, the overwhelming majority (>90 %) of the released particles are calculated to be in the
270 TTL for the previous 12 days, with negligible evidence for transport from the low troposphere. This
271 shows the dominance of the long-range, horizontal transport for the 16-17 and 17-18 km NAME runs
272 (also shown in Navarro et al., 2015).

273 Figure 3 shows the locations at which trajectories crossed 1 km, thereby indicating boundary layer
274 source regions for the RF02 TTL air masses. Boundary layer sources in the West and Central Pacific
275 are the most important for the lowest TTL bin (14-15 km, Fig. 3a) in this flight. The Maritime
276 Continent, the Northern Australia coast, the Indian Ocean and the equatorial band of the African
277 continent increase in relative importance as altitude increases, though the overall contribution of
278 recent boundary layer air masses decreases with increasing altitude.

279 Figure 4 shows the NAME modelled boundary layer contribution to the TTL for CH_3I, $CHBr_3$ and
280 CH_2Br_2 during RF02. It is important to note that this contribution corresponds to uplift from below 1
281 km in the preceding 12 days, the length of the trajectories. The calculated boundary layer
282 contributions for CH_3I, $CHBr_3$ and CH_2Br_2 from the 1 km fractions are highest at 14-15 km,
283 dropping off with altitude. Almost no boundary layer contribution is found for 17-18 km (with values
284 close to 0 ppt).

3.1.2 NAME modelled background contribution

286 Here we explore the two approaches summarised in Sect. 2.3.2 for estimating the $CHBr_3$ and CH_2Br_2
287 background mixing ratios. Similar values are seen in ATTREX 2013 and 2014. Less variation is
288 observed for CH_2Br_2 due to its longer atmospheric lifetime.

289 ATTREX 2013 and 2014 are treated separately in the analysis presented below due to the difference
290 in CH_3I background estimates. The approach using the lowest 10 % of the boundary layer fractions is
291 used to estimate the background contribution for the 2014 flights as not enough data meet the former
292 condition due to the proximity of the flights to strong convection. The background values, inferred
293 from all the ATTREX 2014 flights, are used in the individual flight calculations as again there are
294 not enough data from an individual flight to make background calculations for that flight. In
295 ATTREX 2013 we use the boundary layer fractions less than 5 % approach for the CH_3I background
296 estimation. The ATTREX 2014 background estimates should be taken as upper limits as it is hard to
297 identify samples with no convective influence in 2014. This is especially true for the lower TTL
298 since the ATTREX 2014 flights were close to the region of strong convection.

299 Figure 5 shows the VSL background mixing ratios calculated for the ATTREX campaigns in 2013
300 and 2014. In ATTREX 2013, low CH_3I background mixing ratios are found. All approaches show
301 similar background mixing ratios. In 2014, higher CH_3I background mixing ratios are calculated due
302 to ubiquity of air from recent, vertical uplift. No boundary layer fractions less than 1 % are found for
303 the 14-17 km bins, and less than 5 % for the 14-15 km.

3.1.3 NAME modelled total concentrations

305 The NAME boundary layer and background contribution estimates are added to give an estimate for
306 total halocarbon mixing ratio, $[X]_{NAME\_TTL}$ (Eq. (1)), for comparison with the AWAS observations.

307 Figure 6 and Table 2 show the vertical distribution of NAME-based estimates for CH_3I, $CHBr_3$ and
308 CH_2Br_2 in the TTL for RF02. The sums of the NAME CH_3I, $CHBr_3$ and CH_2Br_2 boundary layer and
309 background contribution estimates agree well with the AWAS observations for all the 1 km TTL
310 bins (compared with Fig. 1).

311 At 14-15 km, the modelled boundary layer contribution of CH_3I is similar to the observations,
312 indicating recent, rapid convective uplift. This provides evidence that the improved convection
313 scheme provides a realistic representation of particle displacement via deep convection. At higher
314 altitudes, the background contribution is more important and, indeed, the modelled total CH_3I values
315 are greater than the observations. This overestimate of the background contribution results from the
316 difficulty of identifying samples with no convective influence in ATTREX 2014. This problem is
317 most important for CH_3I with its very short lifetime.

318 $CHBr_3$ drops off slower with altitude than CH_3I and quicker than CH_2Br_2. At 14-15 km, the
319 boundary layer contribution accounts for ~ 50 % of the modelled sums of $CHBr_3$ and CH_2Br_2, but
320 less than 5 % for $CHBr_3$ and CH_2Br_2 at 17-18 km. For the upper TTL, the background contribution
321 estimates constitute over 85 % of the modelled sums, thus taking on more importance.

322

4 The role of transport in the VSL halocarbon distribution in the TTL

324 The role of transport in the CH_3I, $CHBr_3$ and CH_2Br_2 distribution in the TTL is examined in this
325 section by applying the NAME based analysis introduced in Sect. 3 to all CH_3I, $CHBr_3$ and CH_2Br_2
326 AWAS observations in the ATTREX 2013 and 2014 campaigns.

327 In ATTREX 2013, six flights surveyed the East Pacific TTL in February-March 2013. Four flights
328 went west from Dryden Flight Research Centre to the area south of Hawaii, reaching 180° longitude.
329 Little influence of convective activity was observed. Most samples with strong boundary layer
330 influence were observed in air masses that had originated over the West Pacific and the Maritime
331 Continent, where it was uplifted to the TTL and transported horizontally within the TTL (Navarro et
332 al., 2015). Two flights sampled the TTL near the Central and South American coast. Few convective
333 episodes were observed. The sampled air had predominantly a small boundary layer air signature
334 from the West Pacific and the Maritime Continent.

335 In ATTREX 2014, two transit flights and six research flights were made in the West Pacific in
336 January-February 2014. This period coincided with the active phase of Madden-Julian Oscillation
337 (MJO) and increased activity of tropical cyclones. A large influence of recent convective events is
338 observed (Navarro et al., 2015), reflected in the elevated CH_3I and $CHBr_3$ mixing ratios and the high
339 values of NAME fractions of trajectories below 1 km. All three aircraft flew together in 2014 and so
340 there is a more complete set of measurements from the ground up. Accordingly, this year is
341 discussed first.

4.1 VSL halocarbon distribution in the TTL: ATTREX 2014

343 Figure 7 shows the vertical distribution of the observations and of the modelled boundary layer
344 contribution and total mixing ratios for CH_3I, $CHBr_3$ and CH_2Br_2 for all the ATTREX 2014 flights
345 (using only the AWAS measurements made from 20° N southward). As in RF02, CH_3I is highest in
346 the lower TTL, dropping off with altitude. Large flight-to-flight variability in CH_3I measurements is
347 seen. The fraction of NAME particles that travel below 1 km in the previous 12 days (Table 3) are
348 highest at 14-15 km (mean of 57 %) and decrease with altitude in a similar fashion. The CH_3I
349 boundary layer contribution explains most of the observations for the 14-15 and 15-16 km layers.
350 Disparities in observed and modelled CH_3I arise from 16 km up. Estimated background values are
351 very low, oscillating between 0 and the limit of detection of the AWAS instrument for the iodinated
352 short-lived organic substances, 0.01 ppt. The sums of the CH_3I boundary layer and background

353 contribution estimates show good agreement with AWAS observations for all the TTL 1 km
354 segments (Table 3).

355 The good agreement for the 14-15 km and 15-16 km layers can be attributed to the improved
356 representation of deep convection in NAME, provided by the new convection scheme (Meneguz et
357 al., 2019). However, there is an underestimation of the boundary layer contribution to the upper TTL
358 levels (16-17 and 17-18 km) which we attribute to the new convection scheme not working as well at
359 these altitudes. This is consistent with a known tendency of the Unified Model to underestimate the
360 depth of deepest convection in the tropics (Walters, et al., 2019). Both the CH_3I AWAS observations
361 and the modelled sums are higher than reported previously in the literature (Carpenter et al., 2014)
362 for all the TTL segments. This may be explained by sampling the TTL in a region of high convective
363 activity. This result gives confidence in the quality of the new convection scheme and hence in
364 similar calculations of convective influence on the longer-lived $CHBr_3$ and CH_2Br_2.

365 The highest $CHBr_3$ and CH_2Br_2 concentrations were observed in the lower TTL (14-15 km),
366 dropping off more slowly with altitude than CH_3I. The weight of the modelled boundary layer
367 contribution estimates to the modelled total amounts varies from approximately 50% at 14-15 km
368 (unlike for CH_3I where over 85 % of the modelled sum is attributed to the boundary layer
369 contribution at 14-15 km) to < 20% at 17-18 km. The sums of the modelled boundary layer and
370 background contributions are in good agreement with the $CHBr_3$ and CH_2Br_2 AWAS observations.
371 The ATTREX observations and the NAME modelled sums are within the range of values reported in
372 the literature (Carpenter et al., 2014).

4.2 VSL halocarbon distribution in the TTL: ATTREX 2013

374 Figure 8 shows the vertical distribution for CH_3I, $CHBr_3$ and CH_2Br_2 in the TTL, observed and
375 modelled from the ATTREX 2013 flights. Only AWAS measurements taken south of 20^oN are used.
376 Much lower CH_3I values are found in 2013 than in 2014 (Fig. 7). The NAME 1 km fractions are
377 considerably lower (~fourfold), and the corresponding CH_3I boundary layer contribution shows
378 values close to the limit of detection of the AWAS instrument for CH_3I. The background
379 contribution comprises over 85-90 % of the sums of the modelled CH_3I estimate in the TTL. Good
380 agreement is found between the AWAS observations and the sum of the modelled boundary layer
381 and background contributions. Both the observed and modelled values are in the low end of the CH_3I
382 concentrations reported by the WMO 2014 Ozone Assessment (Carpenter et al., 2014).

383 The ATTREX 2013 mixing ratios are lower for $CHBr_3$ and higher CH_2Br_2 than shown in Fig. 7 for
384 2014. The NAME calculated $CHBr_3$ and CH_2Br_2 boundary layer contributions are small, constituting
385 approximately 10 % of the NAME modelled sums for 14-15 km, and less for the upper TTL
386 segments. The background contribution estimates comprise over 85 % of the modelled sums. Good
387 agreement is found between the sums of the modelled boundary layer and background contributions
388 and the $CHBr_3$ and CH_2Br_2 AWAS observations.

4.3 ATTREX 2013 and 2014: Inter-campaign comparison

390 Clear differences in the vertical distributions of CH_3I in the TTL are found in ATTREX 2013 and
391 2014. CH_3I estimates, corresponding to high values in the NAME modelled 1 km fractions, are high
392 in 2014, whereas in 2013 almost no CH_3I is estimated to be in the TTL. This is due to the minimal
393 contribution of the boundary layer air within the previous 12 days: ATTREX 2013 was in the East
394 Pacific away from the main region of strong convection. Longer transport timescales result from
395 horizontal transport and were more important in ATTREX 2013, with much less recent convective
396 influence than in ATTREX 2014. More chemical removal of CH_3I and $CHBr_3$ thus took place,
397 leading to lower concentrations in the East Pacific TTL.

398 The trajectories are analysed to investigate the timescales for vertical transport by calculating how
399 long it took particles to go from below 1 km to the TTL. In 2013, almost no episodes of recent rapid
400 vertical uplift are found, with most particles taking 8 days and more to cross the 1 km. This is

401 indicative of the dominant role of long-range horizontal transport. In 2014, by way of contrast, a
402 considerable number of trajectories (10's of per cent) come from below 1 km in less than 4 days,
403 representing the 'young' air masses being brought from the low troposphere via recent and rapid
404 vertical uplift.

405 The spatial variability in the boundary layer mixing ratios corresponding to different source strengths
406 coupledled with the variation in atmospheric transport pathways and transport timescales can explain
407 the differences in the distribution of the NAME 1 km fractions in the TTL. In 2014 (2013), higher
408 (lower) boundary layer fractions corresponded well with higher (lower) CH_3I and $CHBr_3$ values in
409 the TTL, especially with the highest concentrations occurring for the flights with the most convective
410 influence and the highest fractions of particles arriving within the 4 days.

411 In 2014 , the western and central Pacific is the dominant source origin of boundary layer air to the
412 TTL (Navarro et al., 2015). Increased tropical cyclone activity in this area (particularly Faxai 28
413 February – 6 March 2014 and Lusi 7-17 March 2014) and the strong signal from the Madden Julian
414 Oscillation (MJO - an intraseasonal phenomenon characterised by an eastward spread of large
415 regions of enhanced and suppressed tropical rainfall, mainly observed over the Indian and Pacific
416 Ocean) related convection contributed to the more frequent episodes of strong and rapid vertical
417 uplifts of the low-level air to the TTL. A significant contribution is also seen from the central Indian
418 Ocean, marking the activity of the Fobane tropical cyclone (6-14 February 2014). Minimal
419 contribution from the other remote sources (Indian Ocean, African continental tropical band) is
420 found (Anderson et al., 2016; Jensen et al., 2017; Newton et al., 2018).

421 **5 How much do VSL bromocarbons contribute to the bromine budget in the TTL?**

422 The NAME modelled $CHBr_3$ and CH_2Br_2 estimates in the TTL are used to calculate how much
423 bromine from the VSL bromocarbons, $Br-VSL_{org}$, is found in the lower stratosphere, based on how
424 much enters the TTL in the form of bromocarbons (Navarro et al. (2015)). $CHBr_3$ and CH_2Br_2 are
425 the dominant short-lived organic bromocarbons, and the minor bromocarbons: CH_2BrCl, $CHBr_2Cl$
426 and $CHBrCl_2$ are excluded here (their combined contribution is less than 1 ppt to $Br-VSL_{org}$ at 14-18
427 km, Navarro et al., 2015). The NAME modelled $CHBr_3$ and CH_2Br_2 estimates are multiplied by the
428 number of bromine atoms (bromine atomicity), and then summed to yield the total of $Br-VSL_{org}$.

429 Figure 9 shows the contribution of $CHBr_3$ and CH_2Br_2, the two major VSL bromocarbons
430 contributing to the bromine budget in the TTL. For ATTREX 2013 and 2014, similar contributions
431 of $CHBr_3$ and CH_2Br_2 to $Br-VSL_{org}$ are found in the lower TTL. In 2014, $CHBr_3$ in the lower TTL
432 was abundant enough to contribute as much $Br-VSL_{org}$ as CH_2Br_2. A combination of larger boundary
433 layer air influence in the TTL and shorter mean transport times to reach the TTL result in the
434 observed higher $CHBr_3$ contribution to the $Br-VSL_{org}$ in the lower TTL in 2014, than in 2013. The
435 CH_2Br_2 contribution dominates in the upper TTL due to its longer atmospheric lifetime.

436 Good agreement is found between the bromine loading from the VSL bromocarbons, inferred from
437 the NAME modelled estimates initialised with BAe-146 and GV measurements, and the Global
438 Hawk AWAS observations. Higher organic bromine loading is seen around the cold point tropopause
439 (16-17 km) in ATTREX 2014.

440 Using the upper troposphere measurements taken during the SHIVA campaign in the western Pacific
441 in November-December 2011, Sala et al. (2014) calculated an estimate for VSLS ($CHBr_3$, CH_2Br_2,
442 $CHBrCl_2$, CH_2BrCl, $CHBr_2Cl$) contribution to the organic bromine at the level of zero radiative
443 heating (15.0 - 15.6 km). Air masses reaching this level are expected to reach the stratosphere. This
444 VSLS mean mixing ratio estimate of 2.88 (+/- 0.29) ppt (2.35 ppt for $CHBr_3$ and CH_2Br_2, excluding
445 minor short-lived bromocarbons) is lower due to a lower contribution from $CHBr_3$ estimate (0.22 ppt
446 compared to the $CHBr_3$ estimate for NAME / ATTREX in Table 5). Our estimates of the
447 contribution of $CHBr_3$ and CH_2Br_2 to the organic bromine at the LZRH are slightly higher largely
448 than those in Sala et al. (2014) due to a higher estimate for a shorter-lived $CHBr_3$.

449 Several papers use the same measurements from the combined ATTREX/CAST/CONTRAST
450 campaign in 2014 and from the other ATTREX phases. Navarro et al. (2015) report slightly higher
451 bromine loading from the Br-VSL$_{org}$ at the tropopause level (17 km) in the West Pacific, 2014 than
452 in the East Pacific, 2013 (the Br-VSL$_{org}$ values from the AWAS observations were of 3.27 (+/-0.47)
453 and 2.96 (+/-0.42) ppt, respectively). The minor short-lived organic bromine substances were
454 included in the analysis of Navarro et al. (2015), accounting for the higher Br-VSL$_{org}$. Butler et al.
455 (2018), report a mean mole fraction and range of 0.46 (0.13-0.72) ppt and 0.88 (0.71-1.01) ppt of
456 CHBr$_3$ and CH$_2$Br$_2$ being transported to the TTL during January and February 2014. This is
457 consistent with a contribution of 3.14 (1.81-4.18) ppt of organic bromine to the TTL over the region
458 of the campaign. The analysis of the injection of brominated VSLS into the TTL by Wales et al.
459 (2018) using the CAM-chem-SD model combined with a steady state photochemical box model and
460 CONTRAST and ATTREX data found that 2.9 +/- 0.6 ppt of bromine enters the stratosphere via
461 organic source gas injection of VSLS. The NAME modelled results presented here (Fig. 9, Table 5)
462 are thus in good agreement with the values reported by Navarro et al. (2015), Butler et al. (2018) and
463 Wales et.al. (2018).

464

465 **6 Summary and Discussion**

466 We have used the NAME trajectory model in backward mode to assess the contribution of recent
467 convection to the mixing ratios of three short-lived halocarbons, CH$_3$I, CHBr$_3$ and CH$_2$Br$_2$. 15,000
468 back-trajectories are computed for each measurement made with the whole air samples on the NASA
469 Global Hawk in ATTREX 2013 and 2014, and the fraction that originated below 1 km is calculated
470 for each sample. A steep drop-off in this fraction is observed between 14-15 km and 17-18 km. Low
471 level measurements of CH$_3$I, CHBr$_3$ and CH$_2$Br$_2$ from the FAAM BAe-146 and the NCAR GV are
472 used in conjunction with these trajectories and an assumed photochemical decay time to provide
473 estimates of the amount of each gas reaching the TTL from below 1 km. Comparison of these
474 modelled estimates with the CH$_3$I measurements shows good agreement with the observations at the
475 lower altitudes in the TTL values, with less good agreement at altitudes > 16 km, though it should be
476 noted that the amounts are very small here. The lifetime of CH$_3$I is 3-5 days, and so there is a > 90 %
477 decay in the 12 day trajectories. The comparison between the modelled and measured CH$_3$I thus
478 indicates that the NAME convection scheme is realistic up to the lower TTL but less good at
479 reproducing the small number of extreme convective events that penetrate to the upper TTL.

480 In order to perform similar calculations for the longer-lived bromocarbons, an estimate of the
481 background free tropospheric concentration is required. This is found by considering bromocarbon
482 values in samples where there was only a small influence from the boundary layer, i.e. where very
483 few NAME trajectories passed below 1 km. This is possible in 2013 when the ATTREX flights were
484 away from the region of strong convection, but much harder in 2014 when (as planned!) the flights
485 were heavily influenced by convection. By summing the boundary layer and background
486 contributions, an estimate of the total bromocarbon mixing ratio is obtained.

487 The resulting modelled estimates are found to be in generally good agreement with the ATTREX
488 measurements. In other words, a high degree of consistency is found between the low altitude
489 halocarbon measurements made on the BAe-146 and GV and the high altitude measurements made
490 on the Global Hawk when they are connected using trajectories calculated by the NAME dispersion
491 model with its updated convection scheme and driven by meteorological analyses with 25 km
492 horizontal resolution. There are some indications of the modelled convection not always reaching
493 quite high enough, but this is consistent with a known tendency of the Unified Model to
494 underestimate the depth of the deepest convection in the tropics.

495 The resolved winds are likely to be well represented, at least partly because the wind data is analysis
496 rather than forecast data. Hence we expect the main errors in the modelling to arise from the
497 representation of convection. Individual convective events are hard to model and can have significant

498 errors. However because the upper troposphere concentrations depend on a number of convective
499 events and we are considering a range of flights and measurement locations, our conclusions on
500 general behaviour should be robust. The consistency between the aircraft measurements and the
501 NAME simulations supports this.

502 In the above, the boundary layer contribution arises from trajectories which visit the boundary layer
503 within 12 days while the background contribution involves air that has been transported into the TTL
504 from outside the boundary layer on timescales up to 12 days. Sensitivity tests were performed in
505 which the trajectories were followed for longer than 12 days: the effect was to re-allocate some of
506 the air from the background category into the boundary layer contribution with no net change in the
507 total.

508 The approach using NAME trajectories and boundary layer measurements produces Br-VSL$_{org}$
509 estimates of 3.5 +/- 0.4 (3.3 +/- 0.4) ppt in the lower East (West) Pacific TTL (14-15 km) and 2.5 +/-
510 0.2 (2.4 +/-0.4) ppt in the upper East (West) Pacific TTL (17-18 km). These lie within the range of
511 the recent literature findings (Tegtmeier et al., 2012; Carpenter et al., 2014; Liang et al., 2014;
512 Navarro et al., 2015; Butler et al., 2017; Wales et al. 2018). The validation with the ATTREX
513 measurements provides confidence that a similar approach could be used for years when high
514 altitude measurements are not available assuming that realistic estimates of the background
515 tropospheric contributions can be obtained from either models or measurements.

516 Our study of boundary layer contribution of bromoform and dibromomethane into the TTL in the
517 West Pacific, using a combined approach of NAME Lagrangian dispersion modelling and CAST,
518 CONTRAST and ATTREX 2014 measurements, has successfully validated an updated convection
519 scheme for use with the NAME trajectory model. The previous parameterisation scheme was
520 reasonable for convection at mid-latitudes but was far too weak to represent the stronger tropical
521 convection. Comparison with the extensive CH$_3$I measurements made in this campaign provides
522 good support for its use in modelling transport in tropical convective systems. (New scheme:
523 *https://www.harmo.org/conferences/proceedings/_Madrid/publishedSections/H15-29.pdf - please*
524 *note the full paper is accessible upon request – contact Dr David Thomson from the UK Met Office,*
525 *Atmospheric Dispersion and Air Quality Unit).*

526 This represents a considerable improvement on the earlier study by Ashfold et al. (2012) which used
527 the old convection scheme and found reasonable agreement up to and including the level of
528 maximum convective outflow, but not above, when compared to measurements in the East Pacific
529 from CR-AVE and TC4. The approach used by Ashfold et al. (2012) has been further extended so
530 that VSLS mixing ratios can be assigned to contributions from the boundary layer and from the
531 'background' TTL.

532

533 **7 Data availability**

534 The CH$_3$I, CHBr$_3$ and CH$_2$Br$_2$ AWAS data from the NASA ATTREX measurements are available
535 online in the NASA ATTREX database (https://espoarchive.nasa.gov/archive/browse/attrex). The
536 CAST measurements are stored on the British Atmospheric Data Centre, which is part of the Centre
537 for Environmental Data archive at
538 http://catalogue.ceda.ac.uk/uuid/565b6bb5a0535b438ad2fae4c852e1b3. The CONTRAST AWAS
539 data are available through http://catalog.eol.ucar.edu/contrast. The NAME data are available from
540 the corresponding author upon request.

541

542 **8 Author Contribution**

543 The main part of the analysis was conducted by MF. EA and MN provided CH_3I, $CHBr_3$ and CH_2Br_2
544 AWAS measurements from the ATTREX and CONTRAST research flights. SA and LC provided
545 CH_3I, $CHBr_3$ and CH_2Br_2 measurements from the CAST campaign. MA designed initial scripts for
546 NAME runs and products. EM and DT developed the model code for improved convection scheme.
547 MF and NH prepared the manuscript with contributions from all co-authors, NH also supervised this
548 PhD work.

549

9 Acknowledgements

551 The authors would like to thank our NASA ATTREX, NCAR CONTRAST and NERC CAST
552 project partners and the technical teams. MF would like to thank Drs Michelle Cain, Alex Archibald,
553 Sarah Connors, Maria Russo and Paul Griffiths for their input on the NAME applications for flight
554 planning and post-flight modelling. The research was funded through the UK Natural Environment
555 Research Council CAST project (NE/J006246/1 and NE/J00619X/1), and MF was supported by a
556 NERC PhD studentship. EA acknowledges support from NASA grants NNX17AE43G,
557 NNX13AH20G and NNX10AOB3A. We acknowledge use of the NAME atmospheric dispersion
558 model and associated NWP meteorological datasets made available to us by the UK Met Office.

559

10 References

561 Anderson, D.C., Nicely, J.M., Salawitch, R.J., Canty, T.P., Dickerson, R.R., Hanisco, T.F., Wolfe,
562 G.M., Apel, E.C., Atlas, E., Bannan, T., Bauguitte, S., Blake, N.J., Bresch, J.F., Campos, T.L.,
563 Carpenter, L.J., Cohen, M.D., Evans, M., Fernandez, R.P., Kahn, B.H., Kinnison, D.E., Hall, S.R.,
564 Harris, N.R.P., Hornbrook, R.S., Lamarque, J-F., Le Breton, M., Lee, J.D., Percival, C., Pfister, L.,
565 Bradley Pierce, R., Riemer, D.D., Saiz-Lopez, A., Stunder, B.J.B., Thompson, A.M., Ullmann, K.,
566 Vaughan, A., and Weinheimer, A.J.: A pervasive role for biomass burning in tropical high ozone /
567 low water structures, Nature Comms, 7, doi: 10.1038/ncomms10267, 2016.

568 Andrews, S.J., Jones, C.E., and Carpenter, L.J.: Aircraft measurements of very short-lived
569 halocarbons over the tropical Atlantic Ocean, Geophys Res Lett., 40 (5), 1005-1010, doi:
570 10.1002/grl.50141, 2013.

571 Andrews, S.J., Carpenter, L.J., Apel, E.C., Atlas, E., Donets, V., Hopkins, J.R., Hornbrook, R.S.,
572 Lewis, A.C., Lidster, R. T., Lueb, R., Minaeian, J., Navarro, M., Punjabi, S., Riemer, D., and
573 Schauffler, S.: A comparison of very short lived halocarbon (VSLS) and DMS aircraft measurements
574 in the tropical west Pacific from CAST, ATTREX and CONTRAST, Atmos. Meas. Tech., 9, 5213-
575 5225, doi: 10.5194/amt-9-5213-2016, 2016.

576 Ashfold, M.J., Harris, N.R.P., Atlas, E.L., Manning, A.J., and Pyle, J.A.: Transport of short-lived
577 species into the Tropical Tropopause Layer, Atmos. Chem. Phys., 12, 6309-6322, doi: 10.5194/acp-
578 12-6309-2012, 2012.

579 Ball, W.T., Alsing, J., Mortlock, D.J., Rozanov, E.V., Tummon, F., and Haigh, J.D.: Reconciling
580 differences in stratospheric ozone composites, Atmos. Chem. Phys., 17, 12269-12302, doi:
581 10.5194/acp-17-12269-2017, 2017.

582 Ball, W. T., Alsing, J., Staehelin, J., Davis, S. M., Froidevaux, L., and Peter, T.: Stratospheric ozone
583 trends for 1985–2018: sensitivity to recent large variability, Atmos. Chem. Phys. Discuss.,
584 https://doi.org/10.5194/acp-2019-243, in review, 2019.

585 Butler, R., Palmer, P.I., Feng, L., Andrews, S.J., Atlas, E.L., Carpenter, L.J., Donets, V., Harris,
586 N.R.P., Montzka, S.A., Pan, L.L., Salawitch, R.J., and Schauffler, S.M.: Quantifying the vertical
587 transport of $CHBr_3$ and CH_2Br_2 over the Western Pacific, Atmos. Chem. Phys. Discuss., doi:
588 10.5194/acp-2016-936, 2016.

589 Carpenter, L. J., Sturges, W. T., Penkett, S. A., Liss, P. S., Alicke, B., Hebestreit, K., and Platt, U.,
590 Short-lived alkyl iodides and bromides at Mace Head, Ireland: Links to biogenic sources and halogen
591 oxide production, J. Geophys. Res., 104, 1679, 1999.

592 Carpenter, L.J., Archer, S.D., and Beale, R.: Ocean-atmosphere trace gas exchange, Chem. Soc.
593 Rev., 41 (19), 6473-6506, doi: 10.1039/c2cs35121h, 2012.

594 Carpenter, L.J., Reimann, S., Burkholder, J.B., Clerbaux, C., Hall, B.D., Hossaini, R., Laube, J.C.,
595 and Yvon-Lewis, S.A.: Ozone-depleting substances (ODSs) and other gases of interest to the
596 Montreal Protocol, Chap.1, in Scientific Assessment of Ozone Depletion, 2014; Global Ozone
597 Research and Monitoring Project – Report no 55, World Meteorological Organisation, Geneva,
598 Switzerland, 2014.

599 Chipperfield, M.P., Bekki, S., Dhomse, S., Harris, N.R.P., Hassler, B., Hossaini, R., Steinbrecht, W.,
600 Thiéblemont, R., and Weber, M.: Detecting recovery of the stratospheric ozone layer, Nature, 549,
601 211–218, doi: 10.1038/nature23681, 2017.

602 Davies, T., Cullen, M.J.P., Malcolm, A.J., Mawson, M.H., Staniforth, A., White, A.A., and Wood,
603 N.: A new dynamical core for the Met Office's global and regional modelling of the atmosphere, Q.
604 J. Roy. Meteorol. Soc., 131, 1759–1782, doi: 10.1256/qj.04.101, 2005.

605 Dessens, O., Zeng, G., Warwick, N., and Pyle, J.: Short-lived bromine compounds in the lower
606 stratosphere; impact of climate change on ozone, Atmos. Sci. Lett., 10, 201-206, doi:
607 10.1002/asl.236, 2009.

608 Engel, A. and M. Rigby (Lead Authors), J.B. Burkholder, R.P. Fernandez, L. Froidevaux, B.D. Hall,
609 R. Hossaini, T. Saito, M.K. Vollmer, and B. Yao, Update on Ozone-Depleting Substances (ODSs)
610 and Other Gases of Interest to the Montreal Protocol, Chapter 1 in *Scientific Assessment of Ozone*
611 *Depletion: 2018,* Global Ozone Research and Monitoring Project–Report No. 58, World
612 Meteorological Organization, Geneva, Switzerland, 2018.

613 Fernandez, R.P., Salawitch, R.J., Kinnison, D.E., Lamarque, J-F., and Saiz-Lopez, A.: Bromine
614 partitioning in the tropical tropopause layer: Implications for stratospheric injection, Atmos. Chem.
615 Phys., 14, 13391-13410, doi: 10.5194/acp-14-13391-2014, 2014.

616 Fiehn, A., Quack, B., Hepach, H., Fuhlbrügge, S., Tegtmeier, S., Toohey, M., Atlas, E., and Krüger,
617 K.: Delivery of halogenated very short-lived substances from the west Indian Ocean to the
618 stratosphere during the Asian summer monsoon, Atmos. Chem. Phys., 17, 6723-6741,
619 doi:10.5194/acp-17-6723-2017, 2017.

620 Fueglistaler, S., Dessler, A.E., Dunkerton, T.J., Folkins, I., Fu, Q., and Mote, P.W.: Tropical
621 tropopause layer, Reviews of Geophysics, 47 (1), doi:10.1029/2008RG000267, 2009.

622 Fuhlbrügge, S., Quack, B., Tegtmeier, S., Atlas, E., Hepach, H., Shi, Q., Raimund, S., and Krüger,
623 K.: The contribution of oceanic halocarbons to marine and free tropospheric air over the tropical
624 West Pacific, Atmos. Chem. Phys., 16, 7569-7585, doi:10.5194/acp-16-7569-2016, 2016.

625 Harris, N.R.P., Hassler, B., Tummon, F., Bodeker, G.E., Hubert, D., Petropavlovskikh, I.,
626 Steinbrecht, W., Anderson, J., Bhartia, P.K., Boone, C.D., Bourassa, A., Davis, S.M., Degenstein,
627 D., Delcloo, A., Frith, S.M., Froidevaux, L., Godin-Beekmann, S., Jones, N., Kurylo, M.J., Kyrölä,
628 E., Laine, M., Leblanc, S.T., Lambert, J.-C., Liley, B., Mahieu, E., Maycock, A., de Mazière, M.,
629 Parrish, A., Querel, R., Rosenlof, K.H., Roth, C., Sioris, C., Staehelin, J., Stolarski, R.S., Stübi, R.,
630 Tamminen, J., Vigouroux, C., Walker, K.A., Wang, H.J., Wild, J., and Zawodny, J.M.: Past changes
631 in the vertical distribution of ozone – Part 3: Analysis and interpretation of trends, Atmos. Chem.
632 Phys., 15, 9965–9982, doi:10.5194/acp- 15-9965-2015, 2015.

633 Harris, N.R.P., Carpenter, L.J., Lee, J.D., Vaughan, G., Filus, M.T., Jones, R.L., OuYang, B., Pyle,
634 J.A., Robinson, A.D., Andrews, S.J., Lewis, A.C., Minaeian, J., Vaughan, A., Dorsey, J.R.,
635 Gallagher, M.W., Le Breton, M., Newton, R., Percival, C.J., Ricketts, H.M.A., Bauguitte, S.J.-B.,
636 Nott, G.J., Wellpott, A., Ashfold, M.J., Flemming, J., Butler, R., Palmer, P.I., Kaye, P.H., Stopford,

637   C., Chemel, C., Boesch, H., Humpage, N., Vick, A., MacKenzie, A.R., Hyde, R., Angelov, P.,
638   Meneguz, E., and Manning, A.J.: 2017: Coordinated Airborne Studies in the Tropics (CAST), Bull.
639   Amer. Meteor. Soc., 98, 145–162, doi: 10.1175/BAMS-D-14-00290.1, 2017.

640   Hepach, H., Quack, B., Raimund, S., Fischer, T., Atlas, E. L., and Bracher, A.: Halocarbon
641   emissions and sources in the equatorial Atlantic Cold Tongue, Biogeosciences, 12, 6369-6387,
642   https://doi.org/10.5194/bg-12-6369-2015, 2015.

643   Hosking, J.S., Russo, M.R., Braesicke, P. and Pyle, J.A.: Tropical convective transport and the
644   Walker circulation, Atmos. Chem. Phys., 12, 9791-9797, doi: 10.5194/acp-12-9791-2012, 2012.

645   Hossaini, R., Patra, P.K., Leeson, A.A., Krysztofiak, G., Abraham, N.L., Andrews, S.J., Archibald,
646   A.T., Aschmann, J., Atlas, E.L., Belikov, D.A., Bönisch, H., Carpenter, L.J., Dhomse, S., Dorf, M.,
647   Engel, A., Feng, W., Fuhlbrügge, S., Griffiths, P.T., Harris, N.R.P., Hommel, R., Keber, T., Krüger,
648   K., Lennartz, S.T., Maksyutov, S., Mantle, H., Mills, G.P., Miller, B., Montzka, S.A., Moore, F.,
649   Navarro, M.A., Oram, D.E., Pfeilsticker, K., Pyle, J.A., Quack, B., Robinson, A.D., Saikawa, E.,
650   Saiz-Lopez, A., Sala, S., Sinnhuber, B.-M., Taguchi, S., Tegtmeier, S., Lidster, R.T., Wilson, C., and
651   Ziska, F.: A multi-model intercomparison of halogenated very short-lived substances (TransCom-
652   VSLS): linking oceanic emissions and tropospheric transport for a reconciled estimate of the
653   stratospheric source gas injection of bromine, Atmos. Chem. Phys., 16(14), 9163-9187,
654   doi:10.5194/acp-16-9163-2016, 2016.

655   Hossaini, R., Chipperfield, M., Montzka, S.A., Leeson, A.A., Dhomse, S.S., and Pyle, J.A.: The
656   increasing threat to stratospheric ozone from dichloromethane, Nature Comms., doi:
657   10.1038/ncomms15962, 2017.

658   Jensen, E.J., Pfister, L., Jordan, D.E., Bui, T.V., Ueyama, R., Singh, H.B., Thornberry, T.D., Rollins,
659   A.W., Gao, R., Fahey, D.W., Rosenlof, K.H., Elkins, J.W., Diskin, G.S., DiGangi, J.P., Lawson,
660   R.P., Woods, S., Atlas, E.L., Navarro Rodriguez, M.A., Wofsy, S.C., Pittman, J., Bardeen, C.G.,
661   Toon, O.B., Kindel, B.C., Newman, P.A., McGill, M.J., Hlavka, D.L., Lait, L.R., Schoeberl, M.R.,
662   Bergman, J.W., Selkirk, H.B., Alexander, M.J., Kim, J.-E., Lim, B.H., Stutz, J., and Pfeilsticker, K.:
663   The NASA Airborne Tropical Tropopause Experiment: High-Altitude Aircraft Measurements in the
664   Tropical Western Pacific, Bull. Amer. Meteor. Soc., 98, 129–143, doi:10.1175/BAMS-D-14-
665   00263.1, 2017.

666   Jones, A., Thomson, D., Hort, M., and Devenish, B.: The U.K. Met Office's Next-Generation
667   Atmospheric Dispersion Model, NAME III Air Pollution Modeling and Its Application XVII,
668   Springer US, 580-589, doi: 10.1007/978-0-387-68854-1_62, 2007.

669   Krzysztofiak, G., Catoire, V., Hamer, P.D., Marécal, V., Robert, C., Engel, A., Bönisch, H.,
670   Grossman, K., Quack, B., Atlas, E. and Pfeilsticker, K.: Evidence of convective transport in tropical
671   West Pacific region during SHIVA experiment, Atmos. Sci. Lett., 19, 1-7, doi: 10.1002/asl.798,
672   2018.

673   Liang, Q., Stolarski, R.S., Kawa, S.R., Nielsen, J.E., Douglass, A.R., Rodriguez, J.M., Blake, D.R.,
674   Atlas, E.L., and Ott, L.E.: Finding the missing stratospheric Br_y: a global modelling study of $CHBr_3$
675   and CH_2Br_2, Atmos. Chem. Phys., 10, 2269-2286, doi: 10.5194/acp-10-2269-2010, 2010.

676   Liang, Q., Atlas, E., Blake, D., Dorf, M., Pfeilsticker, K. and Schauffler, S.: Convective transport of
677   very short-lived bromocarbons to the stratosphere, Atmos. Chem. Phys. Discuss., 14, 651-676, doi:
678   10.5194/acpd-14-651-2014, 2014.

679   Lovelock, J.E.: Natural halocarbons in the air and in the sea, Nature, 256, 193-194, doi:
680   10.1038/256193a0, 1975.

681   Meneguz, E. and Thomson, D.J.: Towards a new scheme for parametrization of deep convection in
682   NAME III, Int. J. Environ. Pollut., 54, 128-136, doi: 10.1504/IJEP.2014.065113, 2014.

683   Meneguz, E., Filus, M., Selvaratnam, V., Thomson, D. J., Harris, N.P.R., Witham, C. S., Navarro,
684   M. A., and Atlas, E. L.: Improved parametrization scheme to represent tropospheric moist

685 convection in the atmospheric dispersion model NAME, Forecasting Research Technical Report 639,
686 Met Office, United Kingdom, 2019.

687 Moore, R. M., Geen, C. E., and Tait, V. K.: Determination of Henry Law constants for a suite of
688 naturally-occurring halo- genated methanes in seawater, Chemosphere, 30, 1183–1191, 1995.

689 Navarro, M.A., Atlas, E.A., Saiz-Lopez, A., Rodriguez-Lloveras, X., Kinnison, D.E., Lamarque, J.-
690 F., Tilmes, S., Filus, M., Harris, N.R.P., Meneguz, E., Ashfold, M.J., Manning, A.J., Cuevas, C.A.,
691 Schauffler, S.M., and Donets, V.: Airborne measurements of organic bromine compounds in the
692 Pacific tropical tropopause layer, PNAS., USA, 112, 13789-13793, doi: 10.1073/pnas.1511463112,
693 2015.

694 Newton, R., Vaughan, G., Hintsa, E., Filus, M.T., Pan, L.L., Honomichl, S., Atlas, E., Andrews, S.J.,
695 and Carpenter, L.J.: Observations of ozone-poor air in the tropical tropopause layer, Atmos. Chem.
696 Phys., 18, 5157-5171, doi:10.5194/acp-18-5157-2018, 2018.

697 Oram, D.E. and Penkett, S.A.: Observations in eastern England of elevated methyl iodide
698 concentrations in air of Atlantic origin, Atmos. Environ., 28, 1159-1174, doi: 10.1016/1352-
699 2130(94)90293-3, 1994.

700 Oram, D.E., Ashfold, M.J., Laube, J.C., Gooch, L.J., Humphrey, S., Sturges, W.T., Leedham-
701 Elvidge, E., Forster, G.L., Harris, N.R.P., Mead, M.I., Samah, A.A., Phang, S.M., Ou-Yang, C.-F.,
702 Lin, N.-H., Wang, J.-L., Baker, A.K., Brenninkmeijer, C.A.M., and Sherry, D.: A growing threat to
703 the ozone layer from short-lived anthropogenic chlorocarbons, Atmos. Chem. Phys., 17, 11929-
704 11941, doi: 10.5194/acp-17-11929-2017, 2017.

705 Pan, L.L., Atlas, E.L., Salawitch, R.J., Honomichl, S.B., Bresch, J.F., Randel, W.J., Apel, E.C.,
706 Hornbrook, R.S., Weinheimer, A.J., Anderson, D.C., Andrews, S.J., Baidar, S., Beaton, S.P.,
707 Campos, T.L., Carpenter, L.J., Chen, D., Dix, B., Donets, V., Hall, S.R., Hanisco, T.F., Homeyer,
708 C.R., Huey, L.G., Jensen, J.B., Kaser, L., Kinnison, D.E., Koenig, T.K., Lamarque, J., Liu, C., Luo,
709 J., Luo, Z.J., Montzka, D.D., Nicely, J.M., Pierce, R.B., Riemer, D.D., Robinson, T., Romashkin, P.,
710 Saiz-Lopez, A., Schauffler, S., Shieh, O., Stell, M.H., Ullmann, K., Vaughan, G., Volkamer, R., and
711 Wolfe, G.: The Convective Transport of Active Species in the Tropics (CONTRAST) Experiment,
712 Bull. Amer. Meteor. Soc., 98, 106–128, doi:10.1175/BAMS-D-14-00272.1, 2017.

713 Park, S., Atlas, E.L., Jiménez, R., Daube, B.C., Gottlieb, E.W., Nan, J., Jones, D.B.A., Pfister, L.,
714 Conway, T.J., Bui, T.P., Gao, R.-S., and Wofsy, S.C.: Vertical transport rates and concentrations of
715 OH and Cl radicals in the Tropical Tropopause Layer from observations of CO_2 and halocarbons:
716 implications for distributions of long- and short-lived chemical species, Atmos. Chem. Phys., 10,
717 6669-6684, doi: 10.5194/acp-10-6669-2010, 2014.

718 Pfeilsticker, K., Sturges, W.T., Bosch, H., Camy-Peyret, C., Chipperfield, M.P., Engel, A.,
719 Fitzenberger, R., Muller, M., Payan, S., and Sinnhuber, B.-M.: Lower stratospheric organic and
720 inorganic bromine budget for the arctic winter 1998/1999, Geophys. Res. Lett., 27, 3305-3308, doi:
721 10.1029/2000GL011650, 2000.

722 Pyle, J.A., Ashfold, M.J., Harris, N.R.P., Robinson, A.D., Warwick, N.J., Carver, G.D., Gostlow, B.,
723 O'Brien, L.M., Manning, A.J., Phang, S.M., Yong, S.E., Leong, K.P., Ung, E.H., and Ong, S.:
724 Bromoform in the tropical boundary layer of the Maritime Continent during OP3, Atmos. Chem.
725 Phys., 11, 529-542, doi: 10.5194/acp-11-529-2011, 2011.

726 Russo, M.R., Marécal, V., Hoyle, C.R., Arteta, J., Chemel, C., Chipperfield, M.P., Dessens, O.,
727 Feng, W., Hosking, J.S., Telford, P.J., Wild, O., Yang, X., and Pyle, J.A.:Representation of deep
728 convection in atmospheric models – Part 1: Meteorology and comparison with satellite observations,
729 Atmos. Chem. Phys., 11, 2765-2786, doi: 10.5194/acp-11-2765-2011, 2011.

730 Russo, M.R., Ashfold, M.J., Harris, N.R.P., and Pyle, J.A.: On the emissions and transport of
731 bromoform: sensitivity to model resolution and emission location, Atmos. Chem. Phys., 15, 14031-
732 14040, doi: 10.5194/acp-15-14031-2015, 2015.

Saiz-Lopez, A., Fernandez, R.P., Ordóñez, C., Kinnison, D.E., Gómez-Martin, J.C., Lamarque, J.-F., and Tilmes, S.: Iodine chemistry in the troposphere and its effects on ozone, Atmos. Chem. Phys., 14, 13119-13143, doi: 10.5194/acp-14-13119-2014, 2014.

Sala, S., Bönisch, H., Keber, T., Oram, D.E., Mills, G., and Engel, A.: Deriving an atmospheric budget of total organic bromine using airborne in situ measurements from western Pacific area during SHIVA, Atmos. Chem. Phys., 14, 6903-6923, doi:10.5194/acp-14-6903-2014, 2014.

Schauffler, S.M., Atlas, E.L., Flocke, F., Lueb, R.A., Stroud, V., and Travnicek, W.: Measurements of bromine containing organic compounds at the tropical tropopause, Geophys. Res.Lett., 25, 3,317-320, doi:10.1029/98GL00040, 1998.

Schofield, R., Fueglistaler, S., Wohltmann, I., and Rex, M.: Sensitivity of stratospheric Bry to uncertainties in very short lived substance emissions and atmospheric transport, Atmos. Chem. Phys., 11, 1379–1392, doi:10.5194/acp-11-1379-2011, 2011.

Steinbrecht, W., Froidevaux, L., Fuller, R., Wang, R., Anderson, J., Roth, C., Bourassa, A., Degenstein, D., Damadeo, R., Zawodny, J., Frith, S., McPeters, R., Bhartia, P., Wild, J., Long, C., Davis, S., Rosenlof, K., Sofieva, V., Walker, K., Rahpoe, N., Rozanov, A., Weber, M., Laeng, A., von Clarmann, T., Stiller, G., Kramarova, N., Godin-Beekmann, S., Leblanc, T., Querel, R., Swart, D., Boyd, I., Hocke, K., Kämpfer, N., Maillard Barras, E., Moreira, L., Nedoluha, G., Vigouroux, C., Blumenstock, T., Schneider, M., García, O., Jones, N., Mahieu, E., Smale, D., Kotkamp, M., Robinson, J., Petropavlovskikh, I., Harris, N., Hassler, B., Hubert, D., and Tummon, F.: An update on ozone profile trends for the period 2000 to 2016, Atmos. Chem. Phys., 17, 10675– 10690, doi: 10.5194/acp-17-10675-2017, 2017.

Tegtmeier, S., Krüuger, K., Quack, B., Atlas, E.L., Pisso, I., Stohl, A., and Yang, X.: Emission and transport of bromocarbons: from the West Pacific ocean into the stratosphere, Atmos. Chem. Phys., 12, 10633-10648, doi: 10.5194/acp-12-10633-2012, 2012.

Tegtmeier, S., Krüger, K., Quack, B., Atlas, E., Blake, D.R., Boenish, H., Engel, A., Hepach, H., Hossaini, R., Navarro, M.A., Raimund, S., Sala, S., Shi, Q., and Ziska, F.: The contribution of oceanic methyl iodide to stratospheric iodine, Atmos. Chem. Phys., 13, 11869-11886, doi: 10.5194/acp-13-11869-2013, 2013.

Tegtmeier, S., Ziska, F., Pisso, I., Quack, B., Velders, G.J.M., Yang, X., and Krüger, K.: Oceanic bromoform emissions weighted by their ozone depletion potential, Atmos. Chem. Phys., 15, 13647-13663, doi: 10.5194/acp-15-13647-2015, 2015.

Vogt, R., Sander, R., von Glasow, R. and Crutzen, P.J.: Iodine chemistry and its role in halogen activation and ozone loss in the marine boundary layer: a model study, J. Atmos. Chem., 32, 375-395, doi: 10.1023/A:1006179901037, 1999.

Wales, P.A., Salawitch, R.J., Nicely, J.M., Anderson, D.C., Canty, T.P., Baidar, S., et al.: Stratospheric injection of brominated very short-lived substances: aircraft observations in the Western Pacific and representation in global models., Journal of Geophysical Research: Atmospheres, 123, 5690-5719, https://doi.org/10.1029/2017.JD027978, 2018.

Walters, D., Baran, A. J., Boutle, I., Brooks, M., Earnshaw, P., Edwards, J., Furtado, K., Hill, P., Lock, A., Manners, J., Morcrette, C., Mulcahy, J., Sanchez, C., Smith, C., Stratton, R., Tennant, W., Tomassini, L., Van Weverberg, K., Vosper, S., Willett, M., Browse, J., Bushell, A., Carslaw, K., Dalvi, M., Essery, R., Gedney, N., Hardiman, S., Johnson, B., Johnson, C., Jones, A., Jones, C., Mann, G., Milton, S., Rumbold, H., Sellar, A., Ujiie, M., Whitall, M., Williams, K., and Zerroukat, M.: The Met Office Unified Model Global Atmosphere 7.0/7.1 and JULES Global Land 7.0 configurations, Geosci. Model Dev., 12, 1909—1963, doi: 10.5194/gmd-12-1909-2019, 2019.

Wang, S., Schmidt, J.A., Baidar, S., Coburn, S., Dix, B., Koenig, T.K., Apel, E., Bowdalo, D., Campos, T.L., Eloranta, E., Evans, M.J., DiGangi, J.P., Zondlo, M.A., Gao, R.S., Haggerty, J.A., Hall, S.R., Hornbrook, R.S., Jacob, D., Morley, B., Pierce, B., Reeves, M., Romashkin, P., Ter

781   Schure A., and Volkamer, R.:Active and widespread halogen chemistry in the tropical and
782   subtropical free troposphere, PNAS, 112 (30), 9281-9286, doi:10.1073/pnas.1505142112, 2015.
783   Yang, G.P., Yang, B., Lu, X.L: Spatio-temporal variations of sea surface halocarbon concentrations
784   and fluxes from southern Yellow Sea, Biogeochemistry, 121: 369. https://doi.org/10.1007/s10533-
785   014-0007-x, 2014.
786
787

11 Tables

Table 1. Boundary layer concentrations and atmospheric lifetimes for CH₃I, CHBr₃ and CH₂Br₂ (Carpenter et.al., 2014).

Tracer, [X]	Boundary Layer Concentration, $[X]_{BL}$ [ppt]		Atmospheric Lifetime, τ [days]
	CAST and CONTRAST	Carpenter et al., 2014	
	Mean (Range) Median	Median (Range)	
CH₃I	0.70 (0.16-3.34) 0.65	0.8 (0.3-2.1)	4
CHBr₃	0.83 (0.41-2.56) 0.73	1.6 (0.5-2.4)	15
CH₂Br₂	0.90 (0.61-1.38) 0.86	1.1 (0.7-1.5)	94

Table 2. ATTREX 2014 Research Flight 02: AWAS observations, modelled boundary layer contribution, the modelled total mixing ratios for CH₃I, CHBr₃ and CH₂Br₂. The boundary layer and background fractions means and standard deviations (in brackets) are given based on the measurements and modelled values for the samples collected during the flight.

Altitude [km]	AWAS [ppt]	Modelled Boundary Layer Contribution [ppt]	Modelled Total Mixing Ratio [ppt]
CH₃I			
17-18	0.06 (0.02)	0.00 (0.00)	0.06 (0.02)
16-17	0.09 (0.03)	0.00 (0.00)	0.06 (0.02)
15-16	0.17 (0.03)	0.04 (0.04)	0.12 (0.06)
14-15	0.23 (0.09)	0.17 (0.04)	0.21 (0.08)
CHBr₃			
17-18	0.34 (0.17)	0.01 (0.00)	0.29 (0.15)
16-17	0.42 (0.11)	0.03 (0.01)	0.36 (0.14)
15-16	0.55 (0.06)	0.12 (0.07)	0.48 (0.17)
14-15	0.67 (0.10)	0.35 (0.07)	0.58 (0.13)
CH₂Br₂			
17-18	0.72 (0.02)	0.02 (0.01)	0.71 (0.03)
16-17	0.79 (0.07)	0.06 (0.02)	0.76 (0.06)
15-16	0.83 (0.05)	0.19 (0.09)	0.78 (0.10)
14-15	0.89 (0.05)	0.46 (0.08)	0.84 (0.12)
	Boundary Layer fraction [%]	*Background fraction [%]*	
17-18	2.1 (1.1)	97.9	
16-17	7.2 (2.7)	92.8	
15-16	22.9 (10.0)	77.1	
14-15	53.3 (9.0)	46.7	

Table 3. ATTREX 2014 all flights: AWAS observations, modelled boundary layer contribution, the modelled total mixing ratios for CH₃I, CHBr₃ and CH₂Br₂. The boundary layer and background fractions are also given. Means and standard deviations (in brackets).

Altitude [km]	AWAS [ppt]	Modelled Boundary Layer Contribution	Modelled Total Mixing Ratio [ppt]

	[ppt]		
CH₃I			

	[ppt]		
CH_3I			
17-18	0.04 (0.03)	0.02 (0.03)	0.07 (0.04)
16-17	0.11 (0.10)	0.04 (0.04)	0.09 (0.05)
15-16	0.16 (0.14)	0.09 (0.07)	0.15 (0.08)
14-15	0.17 (0.14)	0.15 (0.08)	0.19 (0.11)
$CHBr_3$			
17-18	0.33 (0.14)	0.06 (0.06)	0.32 (0.16)
16-17	0.48 (0.13)	0.12 (0.09)	0.40 (0.17)
15-16	0.54 (0.13)	0.21 (0.12)	0.50 (0.19)
14-15	0.61 (0.13)	0.31 (0.12)	0.55 (0.16)
CH_2Br_2			
17-18	0.73 (0.06)	0.11 (0.09)	0.73 (0.09)
16-17	0.82 (0.08)	0.19 (0.14)	0.78 (0.15)
15-16	0.84 (0.09)	0.32 (0.16)	0.80 (0.17)
14-15	0.86 (0.07)	0.44 (0.15)	0.84 (0.17)
	Boundary Layer fraction [%]	*Background fraction [%]*	
17-18	12.7 (10.9)	87.3	
16-17	22.3 (16.0)	77.7	
15-16	37.8 (18.8)	62.2	
14-15	51.7 (16.1)	48.3	

Table 4. ATTREX 2013 all flights: AWAS observations, modelled boundary layer contribution, the modelled total mixing ratios for CH₃I, CHBr₃ and CH₂Br₂. The boundary layer and background fractions are also given. Means and standard deviations (in brackets).

Altitude [km]	AWAS [ppt]	Modelled Boundary Layer Contribution [ppt]	Modelled Total Mixing Ratio [ppt]
CH_3I			
17-18	0.03 (0.02)	0.00 (0.00)	0.03 (0.01)
16-17	0.03 (0.02)	0.00 (0.00)	0.03 (0.02)
15-16	0.04 (0.02)	0.01 (0.01)	0.03 (0.03)
14-15	0.04 (0.03)	0.01 (0.01)	0.05 (0.03)
$CHBr_3$			
17-18	0.31 (0.10)	0.01 (0.01)	0.31 (0.09)
16-17	0.39 (0.12)	0.02 (0.02)	0.35 (0.11)
15-16	0.54 (0.15)	0.04 (0.04)	0.49 (0.16)
14-15	0.53 (0.15)	0.07 (0.05)	0.53 (0.18)
CH_2Br_2			
17-18	0.79 (0.08)	0.02 (0.04)	0.78 (0.07)
16-17	0.83 (0.07)	0.04 (0.04)	0.81 (0.07)
15-16	0.90 (0.07)	0.07 (0.06)	0.87 (0.10)
14-15	0.91 (0.08)	0.12 (0.09)	0.89 (0.12)
	Boundary Layer fraction [%]	*Background fraction [%]*	

17-18	1.9 (2.3)	98.1		
16-17	4.7 (4.9)	95.3		
15-16	9.8 (7.9)	90.2		
14-15	14.7 (11.1)	85.3		

809
810
811
812
813 *Table 5. Contribution from the very short-lived bromocarbons: CHBr₃ and CH₂Br₂ to the bromine in the TTL as given by*
814 *modelled estimates and AWAS observations for ATTREX 2014 and 2013. [CHBr₃] and [CH₂Br₂] means are shown only.*

Altitude [km]	$[CHBr_3]$ [ppt]	$[CH_2Br_2]$ [ppt]	Br from $CHBr_3$ [ppt]	Br from CH_2Br_2 [ppt]	$Br\text{-}VSL_{org}$ [ppt]
ATTREX 2014					
NAME					
17-18	0.32	0.73	0.96	1.46	2.42
16-17	0.40	0.78	1.20	1.56	2.76
15-16	0.50	0.80	1.50	1.60	3.10
14-15	0.55	0.84	1.65	1.68	3.33
AWAS					
17-18	0.33	0.73	0.99	1.46	2.45
16-17	0.48	0.82	1.44	1.64	3.08
15-16	0.54	0.84	1.62	1.68	3.30
14-15	0.61	0.86	1.83	1.72	3.55
ATTREX 2013					
NAME					
17-18	0.31	0.78	0.93	1.56	2.49
16-17	0.35	0.81	1.05	1.62	2.67
15-16	0.49	0.87	1.47	1.74	3.21
14-15	0.53	0.89	1.59	1.78	3.37
AWAS					
17-18	0.31	0.79	0.93	1.58	2.51
16-17	0.39	0.83	1.17	1.66	2.83
15-16	0.54	0.90	1.62	1.80	3.42
14-15	0.53	0.91	1.59	1.82	3.41

815
816 **12 Figures**
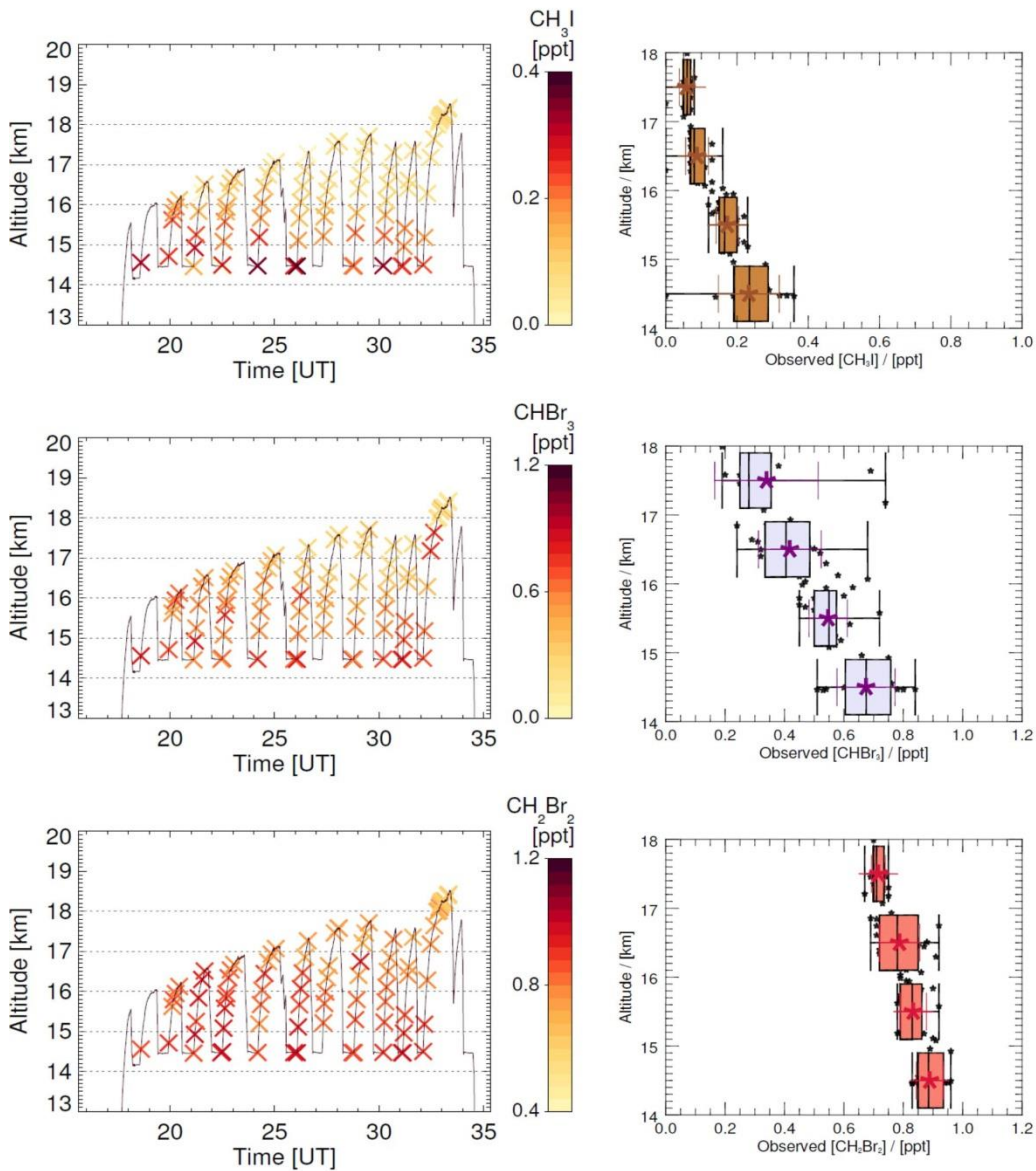
817
818 **Figure 1:** Vertical distribution of CH₃I, CHBr₃ and CH₂Br₂ in the TTL, as measured during research flight 02, ATTREX
819 2014: AWAS measurements along the flight track (left), observations grouped into 1 km TTL segments (right): means
820 (star symbols), standard deviations (coloured whiskers), minimum, lower and upper quartiles, median and maximum
821 (black box and whiskers).
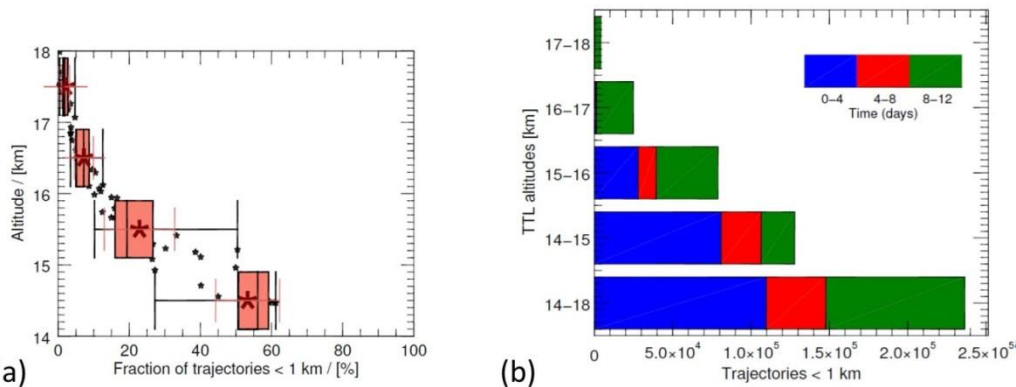
822
823 **Figure 2:** Vertical distribution of NAME 1 km fractions (the fractions which reach the boundary layer within 12 days -
824 indicative of boundary layer air influence) in the TTL (2a, left). Distribution of transport times taken for the trajectories
825 to first cross below 1 km (reach boundary layer) for all the NAME runs and the NAME runs grouped into 1 km TTL
826 segments, research flight 02, ATTREX 2014 (2b, right).
827
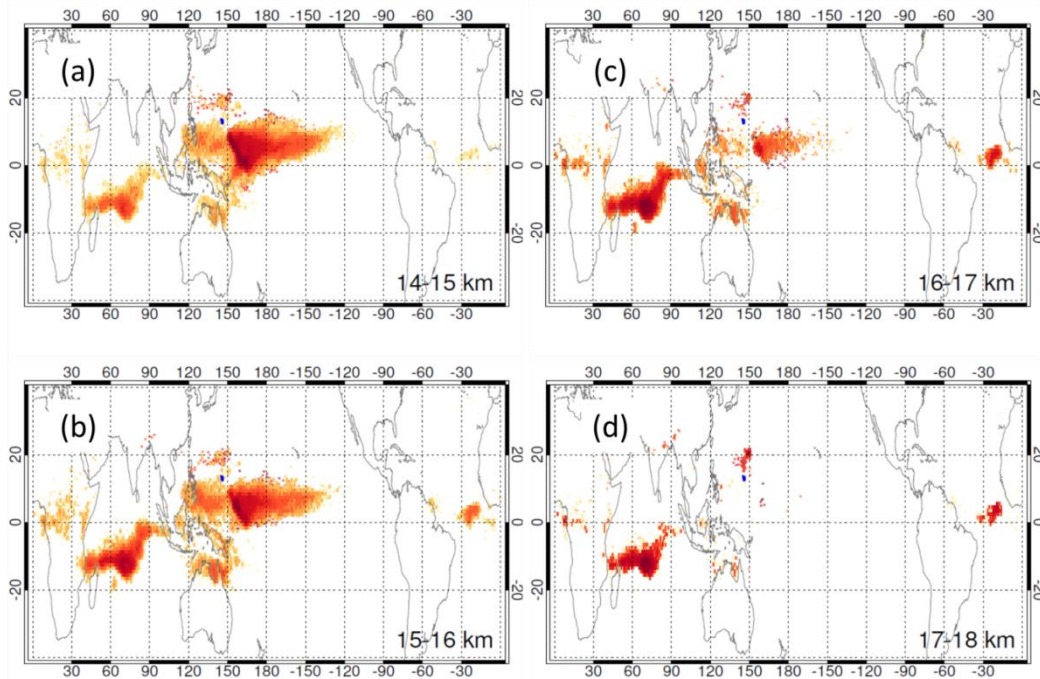
828
829 **Figure 3:** Crossing location distribution maps for all the NAME runs released from 4 1 km TTL altitudes: 14-18 km.
830 Strong influence of local boundary air is noted for a 14-15 km segment (lower TTL), whereas the boundary air from
831 remote locations dominates for a 17-18 km segment (upper TTL), research flight 02, ATTREX 2014.
832
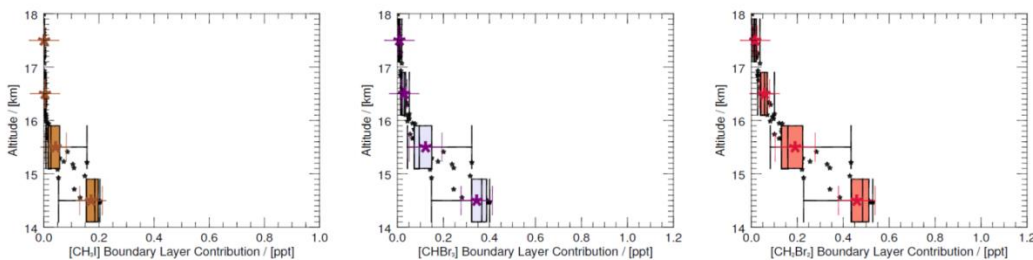
833
834 **Figure 4:** NAME modelled CH$_3$I, CHBr$_3$ and CH$_2$Br$_2$ boundary layer contribution to the TTL, research flight 02,
835 ATTREX 2014.
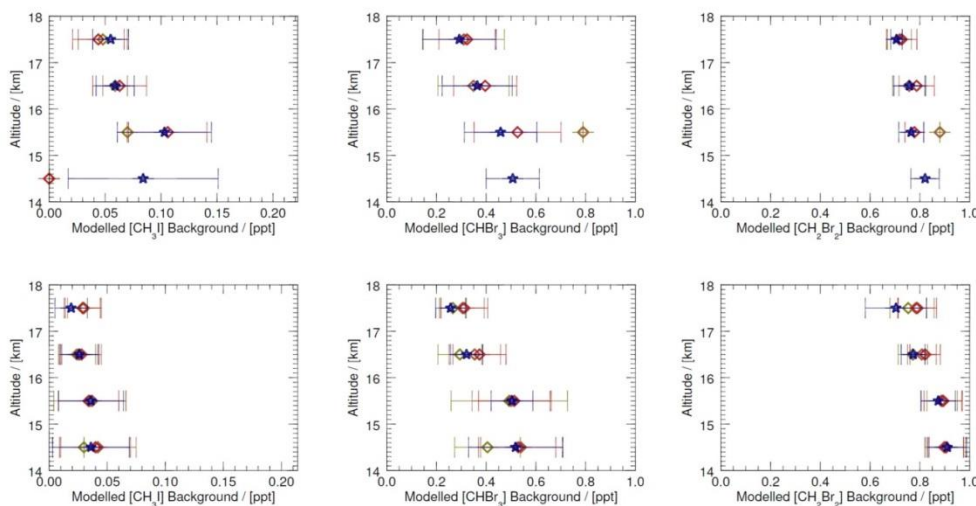
836
837 **Figure 5:** Background mixing ratios for CH$_3$I, CHBr$_3$ and CH$_2$Br$_2$ for all NAME runs for all flights in ATTREX 2014
838 (top row) and ATTREX 2013 (bottom row). Little convective influence is indicated by selecting means from NAME 1
839 km fractions of <1 (blue star), 5 (red diamond) and 10 (green diamond) %.
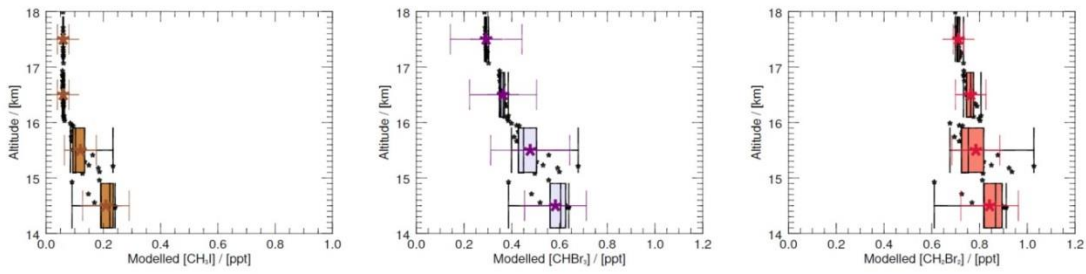
840
841 **Figure 6:** Vertical distribution of NAME modelled CH_3I, $CHBr_3$ and CH_2Br_2 (sums of boundary layer and background
842 contribution) in the TTL for research flight 02, ATTREX 2014.
843
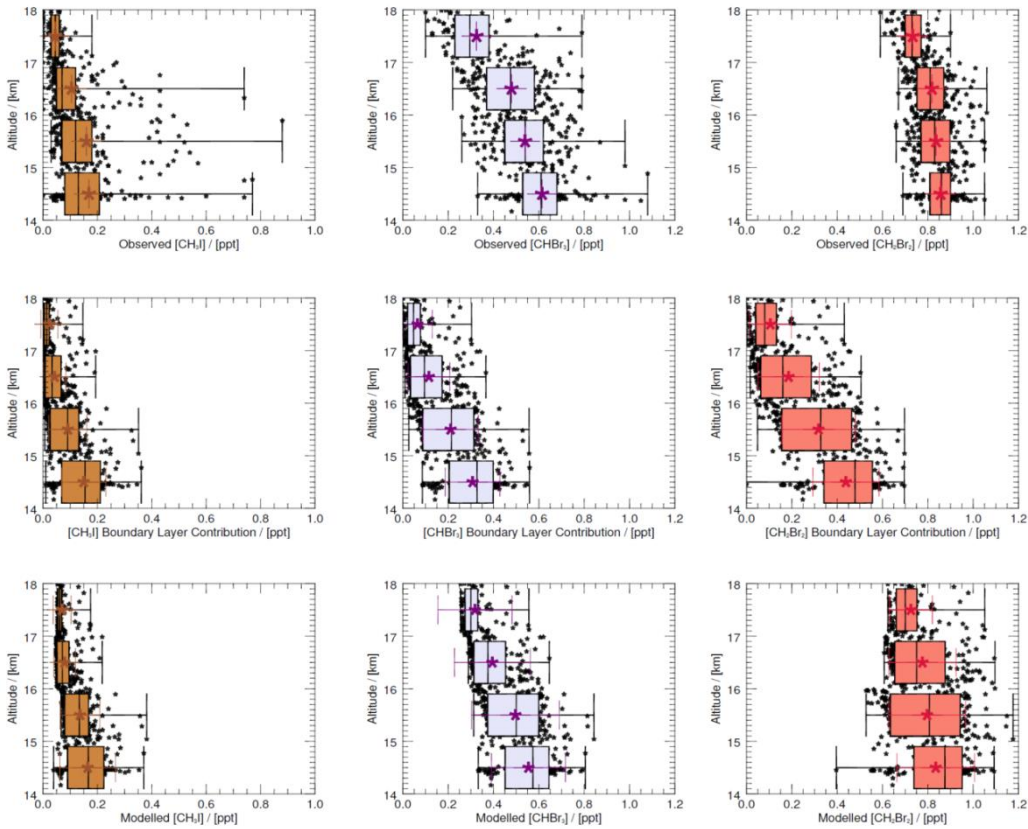
844
845 **Figure 7:** CH_3I, $CHBr_3$ and CH_2Br_2 vertical distribution in the TTL for ATTREX 2014 flights: AWAS observations (top
846 row), NAME modelled boundary layer contribution (middle row), and NAME modelled sums of boundary layer and
847 background contributions (bottom row).
848
849
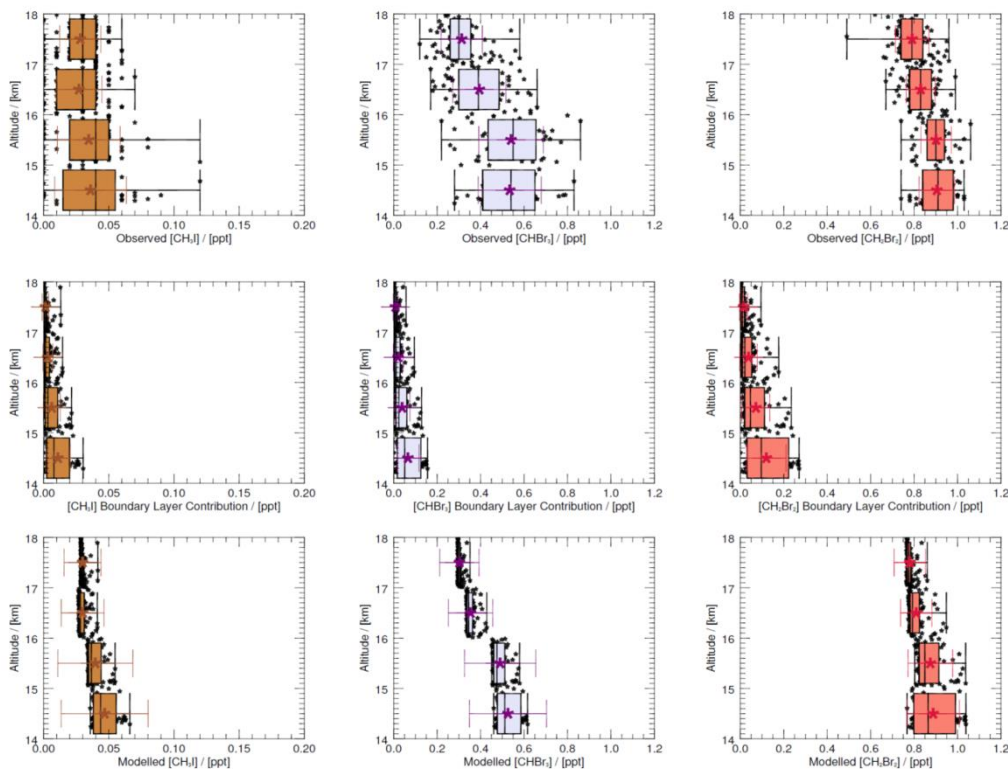
850
851 **Figure 8:** CH$_3$I, CHBr$_3$ and CH$_2$Br$_2$ vertical distribution in the TTL for ATTREX 2013 flights: AWAS observations (top
852 row), NAME modelled boundary layer contribution (middle row), and NAME modelled sums of boundary layer and
853 background contributions (bottom row).
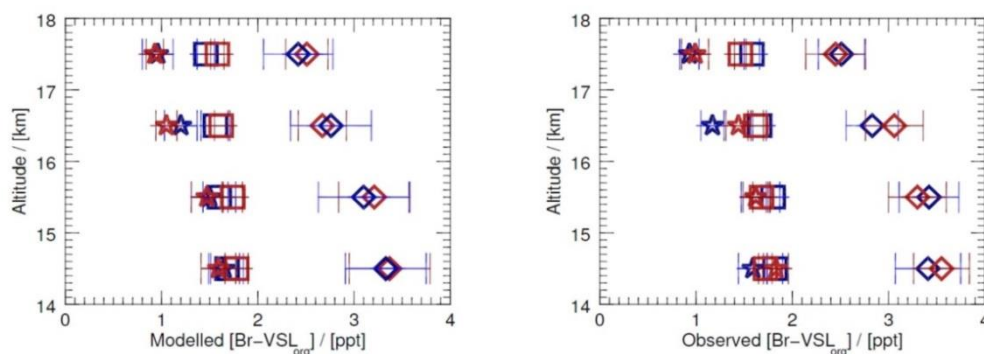
854
855 **Figure 9:** Contribution of CHBr$_3$ (star symbol) and CH$_2$Br$_2$ (square symbol) to the bromine budget in the TTL, inferred
856 from the NAME modelled estimates (left) and AWAS observations (right); separately ATTREX 2014 (red) and 2013
857 (blue). Star and square symbols represent the bromine atomicity products from CHBr$_3$ and CH$_2$Br$_2$, respectively.
858 Diamonds show the bromine contribution from the VSL bromocarbons in the TTL (as a sum of the CHBr$_3$ and CH$_2$Br$_2$
859 bromine atomicity products).
860